Dalton Transactions

ROYAL SOCIETY OF CHEMISTRY

FRONTIER

View Article Online
View Journal | View Issue

Cite this: *Dalton Trans.*, 2025, **54**, 11141

Metal–organic frameworks for purification of methanol-to-olefin (MTO) products

Baobing Tang, Xueyue Yu and Yunling Liu *

Received 13th May 2025,
Accepted 26th June 2025

DOI: 10.1039/d5dt01117e

rsc.li/dalton

Ethylene and propylene are fundamental feedstocks in the chemical industry, and their production currently relies predominantly on petroleum cracking. In recent years, the maturation of methanol-to-olefin (MTO) technology has opened new avenues for the production of low-carbon olefins. Traditionally, separation of MTO products has relied on energy-intensive distillation. The development of physical separation technologies could reduce energy consumption by one-third or more. As an emerging class of crystalline porous materials, metal–organic frameworks (MOFs) exhibit great promise for gas adsorption and separation, owing to their highly tunable pore environments. However, the similar physicochemical properties of MTO products present significant challenges in designing MOF adsorbents with high selectivity for their separation. To date, studies on MOF-based separation of MTO products remain limited. In this review, we provide a concise overview of recent advances in MOF-based adsorbents for the capture and separation of MTO products. We summarize the underlying separation mechanisms and strategies for enhancing MOF performance and finally discuss the remaining challenges and future prospects in this field.

1. Introduction

Ethylene (C_2H_4) and propylene (C_3H_6) are essential building blocks in the modern chemical industry, widely used in the synthesis of polymers, solvents, and a variety of fine chemicals.[1–3] Traditionally, these light olefins are primarily produced *via* steam cracking of petroleum.[4,5] However, with the growing depletion of global petroleum resources and the push toward carbon neutrality, the development of sustainable, non-petroleum-based olefin production technologies has become a major research focus.[6] In recent years, methanol-to-olefin (MTO) technology has emerged as a promising alternative to petroleum cracking for light olefin production, owing to its diverse feedstock options—such as coal, biomass, and CO_2-derived methanol—and excellent product selectivity.[7–9]

The MTO process typically yields approximately 51 wt% of C_2H_4 and 21 wt% of C_3H_6, along with smaller amounts of ethane (C_2H_6), propane (C_3H_8), C_4, and C_5+ hydrocarbons.[10–12] To meet the high-purity requirements of downstream polymerization and fine chemical processes, efficient separation of target olefins from MTO products is essential. However, conventional separation methods rely heavily on cryogenic distillation under high pressure, which is energy-intensive, costly, and demands stringent operational and equipment conditions.[13] As a result, the development of more energy-efficient and cost-effective alternative technologies is key to advancing the industrialization of MTO.

Porous adsorbents, which function through adsorption/desorption cycles, have attracted considerable attention due to their simple operation and low energy consumption, particularly in gas-phase hydrocarbon separations.[14–20] Metal–organic frameworks (MOFs), as a rapidly advancing class of porous materials, offer exceptional advantages in olefin/paraffin separations, owing to their ultra-high surface areas, structural diversity, and tunable pore sizes and surface functionalities.[21–25] In the context of MTO product separation, finely tuned MOFs have demonstrated great potential for highly selective separation of complex multi-component mixtures such as C_3H_6/C_2H_4, C_3H_6/C_2H_6/C_2H_4, and C_3H_6/C_3H_8/C_2H_4.

Nonetheless, the molecular similarity in size and polarity between C_2–C_3 olefins and their corresponding paraffins poses substantial challenges for efficient separation.[26] These challenges necessitate precise control over key structural parameters of MOFs, including pore size matching, pore volume tuning, open metal sites, and N/O/F-containing functional groups.[27–31]

To date, comprehensive reviews on the application of MOFs for MTO product separation remain scarce. This review aims to summarize recent progress in the use of MOFs for separating MTO products—including C_3H_6/C_2H_4, C_3H_6/C_2H_6/C_2H_4, and C_3H_6/C_3H_8/C_2H_4—with a focus on representative MOF structures and their separation performance in practical applications. Furthermore, the key challenges are discussed and

State Key Laboratory of Inorganic Synthesis and Preparative Chemistry, College of Chemistry, Jilin University, Changchun 130012, P. R. China.
E-mail: yunling@jlu.edu.cn

potential future directions are proposed to stimulate deeper research and discussion in this emerging field.

2. Discussion

2.1. C_3H_6/C_2H_4 separation

As the two principal products of the MTO process, the separation of C_3H_6 and C_2H_4 is both fundamental and critical for product purification, offering substantial economic benefits. Although C_3H_6 and C_2H_4 exhibit similar physical properties (Table 1), which poses challenges for their separation, there has been a surge of interest in using MOFs for the separation of C_3H_6/C_2H_4 in recent years. As summarized in Table 2, many MOF materials have demonstrated excellent performance in C_3H_6/C_2H_4 separation, exhibiting significant adsorption capacity and high selectivity.[32–51] MFM-202a reported by Martin Schröder *et al.*, NEM-7-Cu by Wenyue Guo *et al.*, and LIFM-38 by Jijun Jiang *et al.* are among the earliest MOFs developed for C_3H_6/C_2H_4 separation.[46,51,52] With continued advances in MOF research, new materials with superior separation performance have been successively reported. At present, most MOF-based strategies for C_3H_6/C_2H_4 separation are centered on several key design principles, including the use of functionalized organic linkers, the introduction of open metal sites (OMSs), the synergistic integration of OMSs with functionalized linkers, and the construction of single-molecule nanoscopic traps.

Table 1 The physical properties of C_2H_4, C_2H_6, C_3H_6 and C_3H_8

Olefin/paraffin	Molecular dimensions (Å)	Kinetic diameter (Å)	Polarizability $\times 10^{25}$ cm^{-3}	Boiling point (K)
C_2H_4	3.25 × 4.18 × 4.84	4.16	42.5	169.4
C_2H_6	3.81 × 4.08 × 4.44	4.44	44.3–44.7	184.6
C_3H_6	4.20 × 5.30 × 6.40	4.68	62.6	225.5
C_3H_8	4.20 × 4.60 × 6.80	4.30–5.11	62.9–63.7	231.0

2.1.1. Linker functional sites. Co_2(OATA)(DPA), reported by Zhonghua Zhu *et al.*, achieves preferential capture of C_3H_6 through a synergistic combination of optimal pore size and both –NHCO– and –NH– functional groups. At 298 K and 1 bar, it exhibits a C_3H_6 uptake of 121.3 cm^3 g^{-1}—significantly higher than the 94.5 cm^3 g^{-1} uptake for C_2H_4—with a high C_3H_6/C_2H_4 selectivity of 23.1.[32] Notably, Co_2(OATA)(DPA) maintains an exceptionally high C_3H_6 uptake of 97.8 cm^3 g^{-1} even at a low pressure of 0.05 bar. In breakthrough experiments conducted at 298 K, Co_2(OATA)(DPA) was able to produce 97.9 L kg^{-1} of C_2H_4 (99.9% purity) and 75.0 L kg^{-1} of C_3H_6 (99.9%

Table 2 Summary of representative MOFs for C_3H_6/C_2H_4 separation

MOFs	S_{BET} (m^2 g^{-1})	C_3H_6 uptake (cm^3 g^{-1})	C_2H_4 uptake (cm^3 g^{-1})	Q_{st} (C_3H_6) (kJ mol^{-1})	Q_{st} (C_2H_4) (kJ mol^{-1})	C_3H_6/C_2H_4 S_{ads}	Main interactions	Ref.
Co_2(OATA)(DPA)	823	121.3	94.5	28.5	21.7	23.1	C–H···π; C–H···O/N	32
FJI-W9	1026	83	66	38.0	20.9	20.5	C–H···F/O	33
JLU-MOF132	450	52.4	15.8	29.2	25.4	9.2	C–H···F/O	34
Fe-BQDC-BTC-TPBTC	834	69.3	46.2	42.5	28.5	9.6	OMSs	35
FJI-H8-Me	2054	211.0	173.1	44.3	34.3	9.9	C–H···π; C–H···O	36
$Cu_3(OH)_2(Me_2BPZ)_2$	1533	138	52	30.27	20.68	7.4	C–H···π; C–H···O	37
Zn-BPZ-SA	925	68.3	63.9	33.65	23.13	4.8	C–H···π; C–H···O/N/C	38
Mn-dtzip	881	216.4	76.7	32.3	24.2	8.6	OMSs; C–H···O/N	39
1	1958	146.3	47.2	37.6	28.0	9.0	C–H···O/N	40
2	1421	127.3	41.7	34.0	27.3	5.4	C–H···O/N	40
Spe-MOF	3292	236.9	48.9	29.4	22.5	7.7	OMSs; C–H···O/N	41
CoFA	400	92.7	88.0	56.05	33.76	10.43	C═C···H; C═O···H	42
ZJU-74a-Pd[a]	590	108.5	105.7	55.8	30.5	23.4	OMSs; C–H···π; C–H···N≡C/C	43
Fe_2Mn-L	3105	291.1	87.5	39.9	38.9	7.8	OMSs	44
MIL-101(Cr)	2692	196.6	62.1	34.3	35.8	6.6	OMSs	44
ZIF-8	1511	80.6	26.4	29.0	13.8	6.7	OMSs	44
Activated carbon	1086	128.9	98.8	38.5	32.5	11.6	van der Waals	44
HKUST-1	1514	167.0	136.5	48.5	45.1	16.3	OMSs	44
Iso-MOF-1	3211	209.0	51.0	—	—	5.08	OMSs; C–H···π; C–H···O/N	45
Iso-MOF-2	3154	254.1	71.4	—	—	6.60	OMSs; C–H···π; C–H···O/N/F	45
Iso-MOF-3	3067	234.7	66.0	—	—	7.04	OMSs; C–H···π; C–H···O/N	45
Iso-MOF-4	2925	254.5	73.1	30.9	25.4	7.74	OMSs; C–H···π; C–H···O/N/F	45
NEM-7-Cu	786	75.5	29	36.9	22.5	8.6	C–H···O/N	46
CoV-bco-tpt	1042	110.0	102.8	—	—	7.83	van der Waals	47
FDM-201	1965	180.5	68.2	27.1	19.1	8.6	C–H···π; C–H···O/N; π···π	48
SIFSIX-Cu-TPA	—	128.9	26.2[b]	—	—	—	C–H···π; C–H···F; π···π	49
UPC-33	934	94.3	31.1	48.93	10.31	5.7	NH_2 groups	50
LIFM-38	803	58	20	27.3	28.1	6.4	C–H···O/N/F	51
MAF-68	1724	151.9	84.7	31.6	19.9	8.6	C–H···π; π···π	53
JLU-MOF125	1638	148.3	104.8	35.8	26.4	9.7	CH_3 groups	54
JLU-MOF126	1587	130.1	76.6	38.2	21.8	11.0	NH_2 groups	54
UiO-68-2CH_3OCH_3	3133	238.7	58.5	26.2	17.1	6.6	C–H···π	55

[a] 296 K. [b] 10 kPa.

purity) in a single run. GCMC simulations indicate that the primary adsorption mechanism involves C–H···π interactions between C_3H_6 or C_2H_4 and the pyridine moieties of the ligand, as well as C–H···O and C–H···N hydrogen-bonding interactions with the framework. These interactions are generally stronger for C_3H_6 than for C_2H_4. Moreover, it retained high productivity and purity even at 353 K, underscoring its strong potential for application in MTO product separation (Fig. 1).

In 2024, Mingyan Wu *et al.* reported the synthesis of a layered Y-MOF (FJI-W9) assembled from bent diisophthalate ligands and 2-fluorobenzoic acids with Y–O clusters.[33] Benefiting from the exposed –F groups within the pores, FJI-W9 exhibited notable adsorption capacities of 83 $cm^3\ g^{-1}$ for C_3H_6 and 66 $cm^3\ g^{-1}$ for C_2H_4 (298 K, 100 kPa), with a C_3H_6/C_2H_4 IAST selectivity reaching 20.3. GCMC simulations were employed to investigate the adsorption mechanism of FJI-W9, revealing that the preferred adsorption sites for C_3H_6 and C_2H_4 are located around the –F groups and oxygen atoms, where multiple C–H···F/O interactions occur, accompanied by significant differences in static binding energies. Breakthrough experiments confirmed that FJI-W9 can effectively separate C_3H_6/C_2H_4 mixtures and produce polymer-grade C_2H_4, maintaining its separation performance over multiple cycles. These results indicate that FJI-W9 is a promising MOF material for MTO separation.

Yunling Liu *et al.* synthesized a mixed multinuclear cluster-based MOF, JLU-MOF132, using the small V-shaped ligand 2,5-thiophene dicarboxylate.[34] Due to the high connectivity of the multinuclear yttrium clusters, JLU-MOF132 exhibited excellent thermal and solvent stability. After Li^+ ion exchange, the adsorption capacities of C_3H_6 and C_2H_4 at 298 K and 1 bar for JLU-MOF132 were 52.4 $cm^3\ g^{-1}$ and 15.8 $cm^3\ g^{-1}$, respectively, with an IAST selectivity of 9.2 (50/50). In further dynamic breakthrough experiments, JLU-MOF132 demonstrated good separation performance across a wide range of ratios. Under 50/50 (v/v, 298 K) conditions, the C_2H_4 productivity reached 26.1 L kg^{-1}. Under conditions closer to industrial production ratios (20/50, v/v), the C_2H_4 productivity increased to 73.1 L kg^{-1}, surpassing most reported MOFs. In repeated dynamic breakthrough cycles, JLU-MOF132 maintained stable separation performance, and due to its lower Q_{st}, the regeneration conditions for JLU-MOF132 were relatively mild.

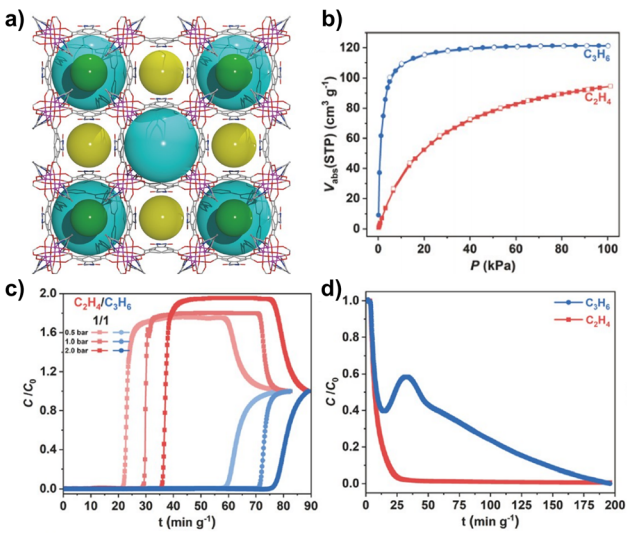

Fig. 1 (a) Three-dimensional framework of Co_2(OATA)(DPA) viewed along the *c*-axis; (b) adsorption isotherms of C_2H_4 and C_3H_6 at 298 K; (c) breakthrough curves for an equimolar C_2H_4/C_3H_6 mixture (1 : 1) at 298 K under varying pressures in Co_2(OATA)(DPA); and (d) desorption profiles of a 1 : 1 C_2H_4/C_3H_6 mixture at 2.0 bar.[32] Reproduced from ref. 32 with permission from Springer Nature, copyright 2024.

2.1.2. Open metal sites. Open metal sites (OMSs) represent a well-established strategy for the selective binding of unsaturated hydrocarbons, as they can form strong π-complexation interactions with unsaturated C=C bonds, thereby imparting MOF materials with exceptional adsorption capabilities.[56,57] In 2024, Bin Li *et al.* synthesized a high-density open-metal-site MOF, ZJU-74a-Pd, featuring sandwich-like nanoscopic traps that are well-matched to C_3H_6 molecules and exhibiting unprecedented binding affinity toward C_3H_6.[43] At 0.1 bar, ZJU-74a-Pd demonstrated an exceptionally high C_3H_6 uptake of 103.8 $cm^3\ g^{-1}$. GCMC simulations revealed that the adsorbed C_3H_6 molecules strongly interact with two adjacent Pd(II) sites, underpinning the high affinity observed. Breakthrough experiments confirmed the excellent performance of ZJU-74a-Pd in separating C_3H_6/C_2H_4 mixtures across various compositions, enabling the production of high-purity C_2H_4 (>99.95%) with a yield of 3.4 mol kg^{-1} in a single-step process. Moreover, the material retained its separation performance over five consecutive cycles. In summary, ZJU-74a-Pd exhibits outstanding performance for C_3H_6/C_2H_4 separation, establishing it as a highly promising MOF candidate for purification of MTO products.

2.1.3. Integration of OMSs and functionalized linkers. In 2019, Daofeng Sun *et al.* synthesized a series of iso-MOFs by employing ligand modification strategies to finely tune the pore environment within the frameworks.[45] Among them, iso-MOF-4 exhibited a maximum C_3H_6 uptake of 254.5 $cm^3\ g^{-1}$ and a C_2H_4 uptake of 73.1 $cm^3\ g^{-1}$ at 298 K and 1 bar, with an IAST selectivity of 7.74. Further GCMC simulations revealed that the exceptionally high C_3H_6 uptake of iso-MOF-4 is attributed to its abundance of phenyl and pyrazine rings, appropriately sized pore spaces, and accessible open metal sites. Further breakthrough experiments confirmed the excellent dynamic separation performance of iso-MOF-4 for C_3H_6/C_2H_4 (298 K, v/v = 50/50), achieving a C_2H_4 productivity of 14.30 mol kg^{-1}. In addition, iso-MOF-4 demonstrated outstanding cycling stability, maintaining its C_2H_4 productivity over multiple adsorption–desorption cycles without significant degradation (Fig. 2).

2.1.4. Single-molecule nanoscopic traps. In 2025, Yuanbin Zhang *et al.* reported a low-cost, easily scalable cobalt formate MOF material, CoFA, for C_3H_6/C_2H_4 separation (Fig. 3).[42] Due to the presence of single-molecule C_3H_6 nano-traps in the CoFA structure, it exhibits preferential adsorption of C_3H_6. Under conditions of 298 K and 1 bar, CoFA synthesized at a 10 g scale had a C_3H_6 adsorption capacity of 94.9 $cm^3\ g^{-1}$,

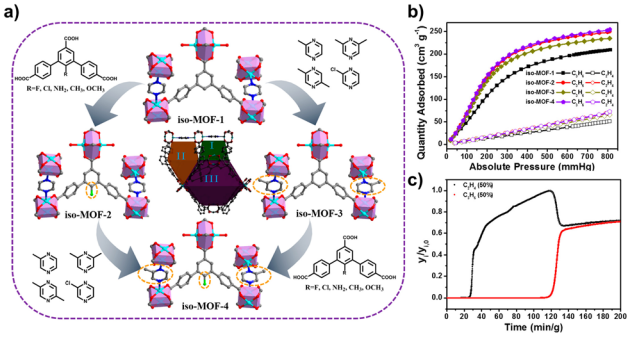

Fig. 2 (a) Structural modulation of iso-MOFs; (b) C_3H_6 and C_2H_4 adsorption isotherms of iso-MOFs at 298 K; and (c) breakthrough curves for a C_3H_6/C_2H_4 gas mixture obtained using iso-MOF-4 at 298 K.[45] Reproduced from ref. 45 with permission from American Chemical Society, copyright 2019.

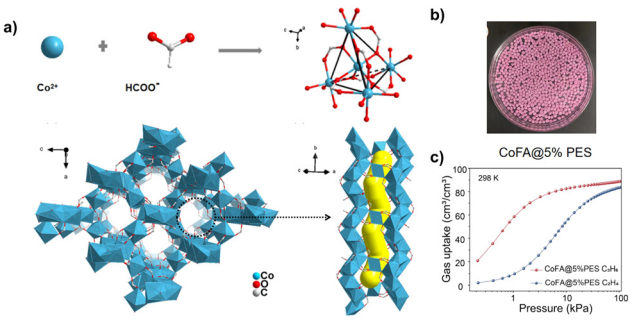

Fig. 3 (a) Structure of CoFA; (b) photographs of CoFA granules after granulation; and (c) adsorption isotherms of C_2H_6 and C_3H_6 on CoFA@5%PES at 298 K and 1 bar.[42] Reproduced from ref. 42 with permission from Elsevier, copyright 2025.

while the C_2H_4 adsorption capacity was 89.3 $cm^3\ g^{-1}$. At 298 K, the IAST selectivity of CoFA for C_3H_6/C_2H_4 was 11.84, which is higher than that of most reported MOF materials used for C_3H_6/C_2H_4 separation. Five dynamic breakthrough experiments were conducted on CoFA under the conditions of C_3H_6/C_2H_4/Ar (10/10/80, v/v/v, 298 K), with an average C_2H_4 productivity of 26.1 ± 2.6 $cm^3\ g^{-1}$, indicating excellent separation performance and good cycling stability. The C_3H_6 and C_2H_4 adsorption capacities of CoFA@5%PES granules, made by using PES as a binder, did not show significant decreases compared to the CoFA powder, indicating their potential for industrial application (Fig. 3). This work provides a low-cost, high-performance MOF material for MTO separation processes.

2.2. $C_3H_6/C_2H_6/C_2H_4$ separation

2.2.1. Nonpolar channels functionalized with N/O/F sites. In actual MTO processes, small amounts of C_2H_6 are present in the product, and the separation of C_2H_6/C_2H_4 is already a highly challenging separation process in MOFs.[58–60] Further separation of $C_3H_6/C_2H_6/C_2H_4$ is undoubtedly even more difficult. Currently, the construction of MOFs capable of separating C_3H_6, C_2H_6, and C_2H_4 primarily relies on avoiding the presence of open metal sites, while incorporating accessible O, N, or F binding sites within the pore environment. This design enables strong binding affinities toward C_3H_6 and C_2H_6 over C_2H_4 through a combination of electrostatic interactions and multiple types of supramolecular binding forces. Table 3 summarizes some representative MOFs for $C_3H_6/C_2H_6/C_2H_4$ separation.[50,52,61–72] In the separation of MTO products, the goal is not only the purification of C_2H_4 but also the recovery of high-purity C_3H_6.

In 2023, Zhonghua Zhu *et al.* designed Zn-BPZ-TATB, featuring active O/N sites and nonpolar pores, to achieve one-step purification of C_2H_4 (99.9%) and recovery of C_3H_6 (99.5%)

Table 3 Summary of representative MOFs for $C_3H_6/C_2H_6/C_2H_4$ separation

MOFs	S_{BET} ($m^2\ g^{-1}$)	C_3H_6 uptake ($cm^3\ g^{-1}$)	C_2H_6 uptake ($cm^3\ g^{-1}$)	C_2H_4 uptake ($cm^3\ g^{-1}$)	C_3H_6/C_2H_4 S_{ads}	C_2H_6/C_2H_4 S_{ads}	Main interactions	Ref.
FJI-Y9	1420	131	105	88	9.6[a]	1.79[b]	OMSs; C–H···π; C–H···O	61
$Zn_2(oba)_2(dmimpym)$	354	76.0	56.4	48.3	15.6	1.8	C–H···π; C–H···O/N/C	62
Zn-BPZ-TATB	1124	114.0	105.1	91.8	7.4	1.7	C–H···π; C–H···O/N/C	63
MAC-4	1218	127	124	83	8.4	2.0	C–H···π; C–H···O/N	64
Al-TCPP	1548	162.4	118.5	101.2	10.1	2.0	C–H···π; C–H···O/N; C···O–H	65
JNU-74a	1006	94.6	82.1	71.5	13.0	2.3	C–H···π; C–H···O/N/F	66
ZJNU-401	1224	101.5	76.8	65.9	15.45	1.75	C–H···π; C–H···O/N	67
$Zn(bdc)(dabco)_{0.5}$	1710	—	—	—	—	—	C–H···π; C–H···O; π···π	68
$Zn(bdc\text{-}Cl)(dabco)_{0.5}$	1723	—	—	—	—	—	C–H···π; C–H···O/Cl; π···π	68
$Zn(bdc\text{-}Cl_2)(dabco)_{0.5}$	1446	—	—	—	3.0	1.7	C–H···π; C–H···O/Cl; π···π	68
$Zn(bdc\text{-}ndc)(dabco)_{0.5}$	1485	—	—	—	—	—	C–H···π; C–H···O; π···π	68
DMOF-1-Cl_2	1222	115.3	110.0	96.8	12.1	1.9	C–H···π; C–H···O/Cl	69
DMOF-1-Br_2	979	85.3	83.4	71.4	11.4	—	C–H···π; C–H···O/Br	69
NKU-0210	1290	180.41	106.10	—	16.4	1.60	C–H···π; C–H···O/N	70
NTUniv-75	889	102	98	97	14.3[a]	1.86[b]	C–H···π; C–H···O/N	71
PL-Co-MOF	1344	135.52	120.05	103.8	8.61	1.49	C–H···π; C–H···O/N	72
MFM-202a	2220	160.8[c]	94.3[c]	65.0[c]	8.4	1.4	C–H···π	52

[a] C_3H_6/C_2H_4 (2/5). [b] C_2H_6/C_2H_4 (10/90). [c] 293 K.

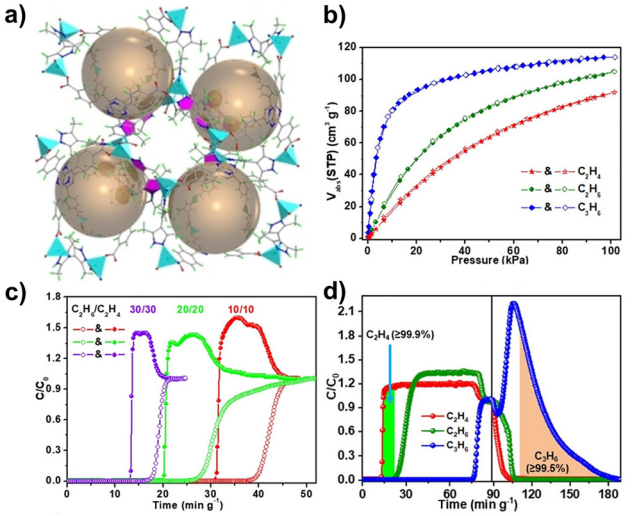

Fig. 4 (a) Structure of Zn-BPZ-TATB; (b) adsorption isotherms for C_2H_4, C_2H_6, and C_3H_6 at 298 K; (c) dynamic breakthrough curves of Zn-BPZ-TATB for C_2H_6/C_2H_4 mixtures with different volume ratios; and (d) dynamic breakthrough and desorption curves of Zn-BPZ-TATB for a $C_2H_6/C_3H_6/C_2H_4$ (5/5/5, v/v/v) mixture.[63] Reproduced from ref. 63 with permission from John Wiley and Sons, copyright 2023.

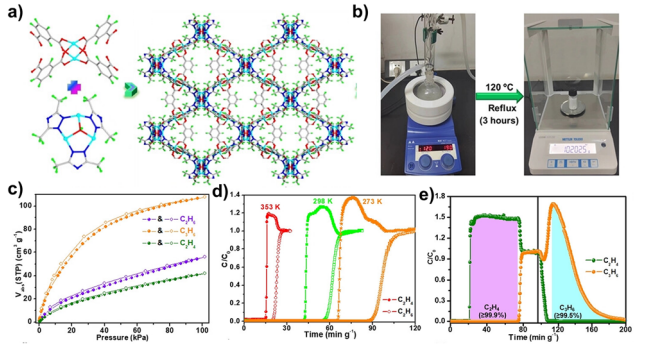

Fig. 5 (a) Structural diagram of MAC-4; (b) large-scale synthesis of MAC-4; (c) adsorption isotherms of C_2H_4, C_2H_6, and C_3H_6 on MAC-4 at 298 K; (d) dynamic breakthrough curves of MAC-4 for a C_2H_6/C_2H_4 mixture (1/1, v/v, 298 K); and (e) dynamic breakthrough and desorption curves of MAC-4 for a $C_2H_6/C_3H_6/C_2H_4$ mixture (5/10/25, v/v/v).[64] Reproduced from ref. 64 with permission from John Wiley and Sons, copyright 2024.

from $C_3H_6/C_2H_6/C_2H_4$ mixtures (Fig. 4).[63] At 298 K and 1 bar, the adsorption capacities of Zn-BPZ-TATB for C_2H_4, C_2H_6, and C_3H_6 are 4.10 mmol g^{-1}, 4.69 mmol g^{-1}, and 5.09 mmol g^{-1}, respectively, indicating that Zn-BPZ-TATB is a selective adsorbent for C_2H_6 and C_3H_6. GCMC simulations were conducted to gain deeper insight into the selective adsorption behavior of Zn-BPZ-TATB. The results reveal that the preferred adsorption sites are primarily located near methyl and carboxyl groups. C_2H_4 forms two C–H···N hydrogen bonds and one C–H···π interaction with the framework, whereas C_2H_6 engages in multiple C–H···C/N/O interactions. In contrast, C_3H_6 exhibits a combination of C–H···π and C–H···C/N/O interactions with the framework. These interactions collectively result in stronger binding affinities for C_2H_6 and C_3H_6 compared to C_2H_4. Further dynamic breakthrough experiments show that Zn-BPZ-TATB can achieve 99.9% C_2H_4 purity from mixtures of C_3H_6 and C_2H_4 at various temperatures (273 K and 298 K) and ratios (10/10, 20/20, and 30/30, v/v). Dynamic breakthrough experiments for a ternary mixture of $C_3H_6/C_2H_6/C_2H_4$, which more closely resembles actual production conditions, show that Zn-BPZ-TATB can produce 99.9% C_2H_4 and obtain 99.5% C_3H_6 after inert gas-assisted thermal desorption, with yields of 38.2 L kg^{-1} and 12.7 L kg^{-1}, respectively.

Another typical example of enhancing the separation of C_3H_6/C_2H_4 and $C_2H_6/C_3H_6/C_2H_4$ through the design of rich O/N sites and nonpolar channels is MAC-4, reported by Lei Hou *et al.* in 2024 (Fig. 5).[64] At 298 K and 1 bar, the adsorption capacities of C_3H_6, C_2H_6, and C_2H_4 on MAC-4 were 127 cm^3 g^{-1}, 107 cm^3 g^{-1}, and 83 cm^3 g^{-1}, respectively, showing preferential adsorption of C_3H_6 and C_2H_6 over C_2H_4. GCMC simulations confirmed that the primary adsorption sites are located within the cavity formed by two $[Zn_2(COO)_4]$ SBUs and two triazolate-trinuclear $[Zn_3(OH)(dmtrz)_3]$ SBUs. Multiple C–H···O/N hydrogen bonds are observed between the ligands and C_2H_4, C_2H_6, and C_3H_6 molecules. However, the interactions between the framework and C_2H_6/C_3H_6 are both more numerous and stronger than those with C_2H_4, consistent with the adsorption behavior of MAC-4. To evaluate its performance in practical separation processes, the dynamic breakthrough curves of MAC-4 for C_2H_6/C_2H_4 and $C_2H_6/C_3H_6/C_2H_4$ mixtures at various temperatures and ratios were further tested (Fig. 5). The experimental results show that MAC-4 exhibited good separation performance. For a $C_2H_6/C_3H_6/C_2H_4$ mixture (2/10/25, v/v/v) at 298 K, MAC-4 produced 27.4 L kg^{-1} of C_2H_4, and after thermal desorption, 36.2 L kg^{-1} of C_3H_6, surpassing most of the reported MOFs. Notably, MAC-4 can be synthesized on a gram scale using inexpensive commercial ligands under heated stirring conditions, making it a potential candidate for industrial adsorption applications.

Dan Li *et al.* enhanced the surface polarity of non-polar pore surfaces by introducing highly electronegative atoms, thereby strengthening binding affinity for C_3H_6 and C_2H_6 over C_2H_4 through a combination of electrostatic interactions and multiple supramolecular binding forces. Based on this strategy, they synthesized a MOF material, JNU-74a, which is rich in O/N/F binding sites.[66] Benefiting from a high density of supramolecular binding sites in its structure, JNU-74a exhibits excellent purification performance for both C_3H_6/C_2H_4 and $C_3H_6/C_2H_6/C_2H_4$ mixtures. Under various dynamic breakthrough conditions, JNU-74a enables the separation of MTO products to yield high-purity C_2H_4 (99.95%), followed by the desorption of high-purity C_3H_6 (99.5%). Notably, in the ternary system, a single adsorption–desorption cycle with JNU-74a yields 12.7 L kg^{-1} of C_2H_4 and 38.2 L kg^{-1} of C_3H_6. More importantly, JNU-74a can be synthesized on a 10-gram scale using relatively inexpensive reagents, making it a promising candidate for the industrial separation of MTO products.

2.3. $C_3H_6/C_3H_8/C_2H_4$ separation

Reports on C_3H_8 separation in the MTO process are currently scarce, mainly due to the limitations in the practical separation performance of MOF-based materials for C_3H_6/C_3H_8 separation, despite the development of various separation mechanisms, including thermodynamic,[74,75] kinetic,[76,77] kinetic-thermodynamic synergy,[78,79] gate effect,[80–85] and molecular sieving.[30] The addition of another product, C_2H_4, further complicates the separation process.

In 2025, Lei Hou *et al.* reported the first MOF material, Cd-dtzip-H_2O, capable of achieving $C_3H_6/C_3H_8/C_2H_4$ separation.[73] This material features a honeycomb-like channel structure, which facilitates the preferential adsorption of C_3H_6 through a vortex effect induced by H_2O in the pores, demonstrating excellent C_3H_6 adsorption performance. At 298 K and 1 bar, the adsorption amount of C_3H_6 reached 112.0 $cm^3\ g^{-1}$, significantly surpassing those of C_3H_8 (66.5 $cm^3\ g^{-1}$) and C_2H_4 (56.7 $cm^3\ g^{-1}$). GCMC simulations revealed that the optimal adsorption sites are located near vortex-like regions formed by water molecules within the framework. The oxygen atoms of the water molecules and the nitrogen atoms in the ligands form multiple C–H···O/N hydrogen bonds with the gas molecules. Among these, C_3H_6 forms a significantly greater number of hydrogen bonds than C_3H_8 and C_2H_4, corroborating the experimental gas adsorption results that indicate a pronounced affinity for C_3H_6. In dynamic experiments, Cd-dtzip-H_2O was able to achieve 5.2 L kg^{-1} of C_3H_6 (99.9%) and 21.7 L kg^{-1} of C_2H_4 (99.5%) in a $C_3H_6/C_3H_8/C_2H_4$ mixture (Fig. 6). Table 4 presents key data on the adsorption behavior of Cd-dtzip-H_2O.[73] Cd-dtzip-H_2O represents a significant step forward in the use of MOFs for the separation of MTO process products, while also presenting greater challenges.

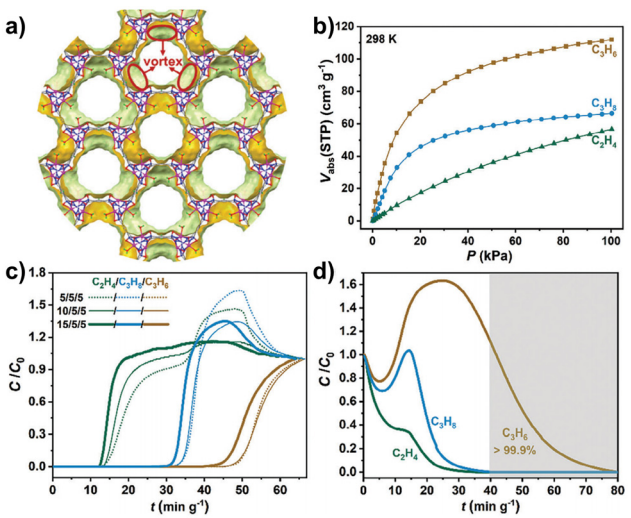

Fig. 6 (a) Pore accumulation diagram of Cd-dtzip-H_2O; (b) gas adsorption isotherms of Cd-dtzip-H_2O at 298 K; (c) breakthrough curves at different ratios of $C_2H_4/C_3H_8/C_3H_6$ mixtures; and (d) desorption curves of $C_2H_4/C_3H_8/C_3H_6$ (15/5/5) mixtures.[73] Reproduced from ref. 73 with permission from John Wiley and Sons, copyright 2025.

3. Conclusion and outlook

As mentioned above, significant progress has been made in the use of MOF materials for MTO product separation, with some MOFs demonstrating excellent performance, highlighting their tremendous potential to replace traditional separation technologies. However, several key challenges remain in further developing efficient and practical MOF materials for industrial MTO separation processes, necessitating in-depth research:

(1) Trade-off between adsorption capacity and selectivity: MOF materials often face a "selectivity-capacity" trade-off during structural design. Some highly selective materials may sacrifice total adsorption capacity, while excessive interaction strength can increase the energy consumption of the regeneration process. These conflicts limit their processing capacity and practical application efficiency. Therefore, achieving high adsorption capacity while maintaining excellent selectivity remains one of the key challenges in the design of MOFs for MTO product separation. Future studies may further explore flexible MOFs, which enable selective adsorption of target molecules through their structural responsiveness, offering the potential for enhanced separation efficiency. In addition, the design and synthesis of kinetically selective MOFs provide a promising strategy for achieving efficient separation of MTO products.

(2) Structural stability: some MOFs, although exhibiting good separation performance under laboratory conditions, may experience rapid performance degradation in practical industrial applications due to structural collapse, deactivation of active sites, or adsorbate competition. Therefore, the development of MOFs with long-term structural stability and good regenerability is essential for advancing their industrial application in MTO product separation. The development of highly stable MOFs with high connectivity, such as Zr-MOFs, represents a promising direction for achieving robust and durable separation of MTO products.

(3) Synthesis cost and scalability: many high-performance MOF materials involve complex precursors and low-yield synthesis routes or are highly sensitive to reaction conditions,

Table 4 Summary of representative MOFs for $C_3H_6/C_3H_8/C_2H_4$ separation

MOFs	S_{BET} ($m^2\ g^{-1}$)	C_3H_6 uptake ($cm^3\ g^{-1}$)	C_3H_8 uptake ($cm^3\ g^{-1}$)	C_2H_4 uptake ($cm^3\ g^{-1}$)	C_3H_6/C_2H_4 S_{ads}	C_3H_6/C_3H_8 S_{ads}	Main interactions	Ref.
Cd-dtzip-H_2O	804	112.0	66.5	56.7	9.0	1.7	C–H···π; C–H···O/N/C	73

severely restricting their large-scale production and engineering applications. Future research should focus on developing green, cost-effective, and scalable synthetic strategies to accelerate the transition of MOF materials for MTO product separation from laboratory studies to practical industrial applications.

(4) Separation behavior in multi-component gas systems: most current research focuses on the separation performance of binary and ternary systems, while MTO products are essentially a complex mixture containing C_2H_4, C_3H_6, C_2H_6, C_3H_8, C_4+, and C_5+. Therefore, the competitive adsorption behavior of MOFs under multi-component conditions, their selectivity retention capabilities, and interactions with impurities all require further systematic investigation.

(5) MTO separation *via* MOF-based membranes: although MOF-based membrane separation technologies have made notable progress in C_2/C_3 separations, research on their application to more complex MTO product mixtures remains relatively limited. In the future, continued advances in the understanding of separation mechanisms and design strategies for MOF membranes are expected to enable efficient separation of multicomponent MTO gas mixtures. This progress will not only contribute to energy savings and emission reductions in low-carbon olefin production, but also lay the groundwork for the practical application of membrane separation technologies in the MTO industry. Further exploration of membrane materials specifically tailored for the complex composition of MTO products represents a critical direction for future research.

Author contributions

Conceptualization: B. T., X. Y. and Y. L.; writing – original draft: B. T. and X. Y.; writing – review & editing: Y. L.; supervision: Y. L.

Conflicts of interest

There are no conflicts to declare.

Data availability

No primary research results, software or code have been included and no new data were generated or analysed as part of this review.

Acknowledgements

This work was supported by the National Natural Science Foundation of China (No. 22171100 and U23A20360) and the '111 Center' (B17020).

References

1 H. Qian, Y. Zhao, F. Qin and G. Song, *Environ. Impact Assess. Rev.*, 2023, **101**, 107152.
2 Y. Jiang, J. Hu, L. Wang, W. Sun, N. Xu, R. Krishna, S. Duttwyler, X. Cui, H. Xing and Y. Zhang, *Angew. Chem., Int. Ed.*, 2022, **61**, e202200947.
3 Z. Di, C. Liu, J. Pang, S. Zou, Z. Ji, F. Hu, C. Chen, D. Yuan, M. Hong and M. Wu, *Angew. Chem., Int. Ed.*, 2022, **61**, e202210343.
4 M. Alabdullah, A. Rodriguez-Gomez, T. Shoinkhorova, A. Dikhtiarenko, A. D. Chowdhury, I. Hita, S. R. Kulkarni, J. Vittenet, S. M. Sarathy, P. Castaño, A. Bendjeriou-Sedjerari, E. Abou-Hamad, W. Zhang, O. S. Ali, I. Morales-Osorio, W. Xu and J. Gascon, *Nat. Catal.*, 2021, **4**, 233–241.
5 F. M. Alotaibi, S. González-Cortés, M. F. Alotibi, T. Xiao, H. Al-Megren, G. Yang and P. P. Edwards, *Catal. Today*, 2018, **317**, 86–98.
6 I. Amghizar, L. A. Vandewalle, K. M. Van Geem and G. B. Marin, *Engineering*, 2017, **3**, 171–178.
7 C. Wang, L. Yang, M. Gao, X. Shao, W. Dai, G. Wu, N. Guan, Z. Xu, M. Ye and L. Li, *J. Am. Chem. Soc.*, 2022, **144**, 21408–21416.
8 S. Wang, Z. Qin, M. Dong, J. Wang and W. Fan, *Chem. Catal.*, 2022, **2**, 1657–1685.
9 X. Yu, B. Tang, Z. Shi, Z. Liu, X. Liu, L. Zhang and Y. Liu, *Sep. Purif. Technol.*, 2025, **366**, 132796.
10 M. Yang, D. Fan, Y. Wei, P. Tian and Z. Liu, *Adv. Mater.*, 2019, **31**, e1902181.
11 P. Tian, Y. Wei, M. Ye and Z. Liu, *ACS Catal.*, 2015, **5**, 1922–1938.
12 A. Cesarini, S. Mitchell, G. Zichittella, M. Agrachev, S. P. Schmid, G. Jeschke, Z. Pan, A. Bodi, P. Hemberger and J. Perez-Ramirez, *Nat. Catal.*, 2022, **5**, 605–614.
13 Q.-Q. Yang, Z.-H. Ma, Q. Zhang, Z.-H. Song, H.-X. Nie, J.-J. Pang, Z.-Q. Yao, H. Huang, M. Feng, T.-L. Hu and J. Xu, *Sep. Purif. Technol.*, 2025, **363**, 132141.
14 C. Gu, N. Hosono, J. J. Zheng, Y. Sato, S. Kusaka, S. Sakaki and S. Kitagawa, *Science*, 2019, **363**, 387–391.
15 H. Zeng, M. Xie, T. Wang, R.-J. Wei, X.-J. Xie, Y. Zhao, W. Lu and D. Li, *Nature*, 2021, **595**, 542–548.
16 H. Zeng, X.-J. Xie, T. Wang, M. Xie, Y. Wang, R.-J. Wei, W. Lu and D. Li, *Nat. Chem. Eng.*, 2024, **1**, 108–115.
17 R. C. Zhao, L. H. Xie, X. M. Liu, Z. Liu, X. Y. Li and J. R. Li, *J. Am. Chem. Soc.*, 2025, **147**, 2467–2475.
18 Y. J. Tian, C. Deng, L. Zhao, J. S. Zou, X. C. Wu, Y. Jia, Z. Y. Zhang, J. Zhang, Y. L. Peng, G. Chen and M. J. Zaworotko, *Nat. Chem.*, 2025, **17**, 141–147.
19 X.-J. Xie, M.-Y. Zhou, H. Zeng, W. Lu and D. Li, *Acc. Mater. Res.*, 2025, **6**, 195–209.
20 Y. Chai, X. Han, W. Li, S. Liu, S. Yao, C. Wang, W. Shi, I. da-Silva, P. Manuel, Y. Cheng, L. D. Daemen, A. J. Ramirez-Cuesta, C. C. Tang, L. Jiang, S. Yang, N. Guan and L. Li, *Science*, 2020, **368**, 1002–1006.
21 Q. Liu, J. Ren, Z. Zhang, H. Li, N. Zhu and D. Zhao, *J. Am. Chem. Soc.*, 2025, **147**, 9273–9282.

22 Y. Z. Hao, K. Shao, X. Zhang, Y. H. Yu, D. Liu, H. M. Wen, Y. Cui, B. Li, B. Chen and G. Qian, *J. Am. Chem. Soc.*, 2025, **147**, 11257–11266.
23 H. M. Wen, C. Yu, M. Liu, C. Lin, B. Zhao, H. Wu, W. Zhou, B. Chen and J. Hu, *Angew. Chem., Int. Ed.*, 2023, **62**, e202309108.
24 D. Liu, J. Pei, X. Zhang, X. W. Gu, H. M. Wen, B. Chen, G. Qian and B. Li, *Angew. Chem., Int. Ed.*, 2023, **62**, e202218590.
25 X. J. Xie, Z. H. Zhang, Q. Y. Cao, Y. L. Huang, D. Luo, H. Zeng, W. Lu and D. Li, *J. Am. Chem. Soc.*, 2024, **146**, 30155–30163.
26 B. Chen, S. Xiang and G. Qian, *Acc. Chem. Res.*, 2010, **43**, 1115–1124.
27 H. C. Zhou, J. R. Long and O. M. Yaghi, *Chem. Rev.*, 2012, **112**, 673–674.
28 J. Li, P. M. Bhatt, J. Li, M. Eddaoudi and Y. Liu, *Adv. Mater.*, 2020, **32**, e2002563.
29 E. D. Bloch, W. L. Queen, R. Krishna, J. M. Zadrozny, C. M. Brown and J. R. Long, *Science*, 2012, **335**, 1606–1610.
30 A. Cadiau, K. Adil, P. M. Bhatt, Y. Belmabkhout and M. Eddaoudi, *Science*, 2016, **353**, 137–140.
31 H. Wang, X. Dong, V. Colombo, Q. Wang, Y. Liu, W. Liu, X. L. Wang, X. Y. Huang, D. M. Proserpio, A. Sironi, Y. Han and J. Li, *Adv. Mater.*, 2018, **30**, e1805088.
32 L. Zhang, J.-Q. Ma, Y.-Z. Guo, X.-Y. Li, L. Hou, Y.-Y. Wang and Z. Zhu, *Sci. China: Chem.*, 2024, **68**, 967–973.
33 H. Li, Y. Zhou, C. Chen, Y. Li, Z. Liu, M. Wu and M. Hong, *Inorg. Chem.*, 2024, **63**, 21548–21554.
34 D. Wang, Z. Shi, W. Li, G. Li, X. Liu and Y. Liu, *Chem. Eng. J.*, 2024, **498**, 155176.
35 Y. Wang, Y.-N. Ma, H.-F. Zhang, J. Yan, T.-L. Liu, M. Li and D.-X. Xue, *Cryst. Growth Des.*, 2024, **24**, 4884–4888.
36 Z. Di, Z. Ji, C. Chen, R. Krishna, D. Yuan, M. Hong and M. Wu, *Chem. Eng. J.*, 2024, **493**, 152442.
37 G. Zhen, Y. Liu, Y. Zhou, Z. Ji, H. Li, S. Zou, W. Zhang, Y. Li, Y. Liu, C. Chen and M. Wu, *ACS Appl. Mater. Interfaces*, 2024, **16**, 1179–1186.
38 G.-D. Wang, R. Krishna, Y.-Z. Li, Y.-Y. Ma, L. Hou, Y.-Y. Wang and Z. Zhu, *ACS Mater. Lett.*, 2023, **5**, 1091–1099.
39 L. Zhang, L.-N. Ma, G.-D. Wang, L. Hou, Z. Zhu and Y.-Y. Wang, *J. Mater. Chem. A*, 2023, **11**, 2343–2348.
40 W.-Q. Wei, X.-A. Guo, Z.-H. Zhang, Y.-F. Zhang and D.-X. Xue, *Inorg. Chem. Commun.*, 2021, **133**, 108896.
41 H. Fang, B. Zheng, Z. H. Zhang, H. X. Li, D. X. Xue and J. Bai, *Angew. Chem., Int. Ed.*, 2021, **60**, 16521–16528.
42 S. Chen, X. Li, Y. Hu, Y. Jiang, J. Hu, C. Liu, L. Wang, Y. He and Y. Zhang, *Sep. Purif. Technol.*, 2025, **359**, 130638.
43 J.-X. Wang, T.-F. Zhang, J. Pei, D. Liu, Y.-B. Wang, X.-W. Gu, G. Qian and B. Li, *Chem Bio Eng.*, 2024, **1**, 952–959.
44 X. M. Liu, L. H. Xie and Y. Wu, *Materials*, 2023, **16**, 154.
45 W. Fan, X. Wang, X. Zhang, X. Liu, Y. Wang, Z. Kang, F. Dai, B. Xu, R. Wang and D. Sun, *ACS Cent. Sci.*, 2019, **5**, 1261–1268.
46 X. Liu, C. Hao, J. Li, Y. Wang, Y. Hou, X. Li, L. Zhao, H. Zhu and W. Guo, *Inorg. Chem. Front.*, 2018, **5**, 2898–2905.
47 Y. Xiao, A. N. Hong, Y. Chen, H. Yang, Y. Wang, X. Bu and P. Feng, *Small*, 2023, **19**, e2205119.
48 Y. Rao, X. Li, H. Xi, Z. Jiang, W. Li, H. Zhou, Y. Zhang, C. Wu, Y.-B. Zhang and Q. Li, *J. Mater. Chem. A*, 2025, **13**, 11382–11388.
49 Z. Ji, Y. Zhou, Y. Zhu, Y. Liu, Z. Di, M. Hong and M. Wu, *ACS Mater. Lett.*, 2025, **7**, 837–844.
50 W. Fan, Y. Wang, Q. Zhang, A. Kirchon, Z. Xiao, L. Zhang, F. Dai, R. Wang and D. Sun, *Chemistry*, 2018, **24**, 2137–2143.
51 C.-X. Chen, Z.-W. Wei, Q.-F. Qiu, Y.-Z. Fan, C.-C. Cao, H.-P. Wang, J.-J. Jiang, D. Fenske and C.-Y. Su, *Cryst. Growth Des.*, 2017, **17**, 1476–1479.
52 S. Gao, C. G. Morris, Z. Lu, Y. Yan, H. G. W. Godfrey, C. Murray, C. C. Tang, K. M. Thomas, S. Yang and M. Schröder, *Chem. Mater.*, 2016, **28**, 2331–2340.
53 Y. G. Li, J. X. Chen, J. H. Li, W. X. Zhou, L. Li, J. Li, R. B. Lin, J. P. Zhang and X. M. Chen, *Small*, 2025, e2504613, DOI: **10.1002/smll.202504613**.
54 J. Li, Z. Shi, X. Liu, L. Zhang and Y. Liu, *ACS Mater. Lett.*, 2025, **7**, 2063–2070.
55 H.-O. Qi, F. Li, H.-D. Li, X.-Q. Liu, G. Liu and L.-B. Sun, *Sep. Purif. Technol.*, 2025, **367**, 132848.
56 R. Zhang, Y. Fan, J.-p. Xue, Y. Chai, B. Li and J. Li, *Inorg. Chem. Front.*, 2025, DOI: **10.1039/D5QI00788G**.
57 Y. Z. Hao, H. M. Wen, Y. H. Yu, X. Zhang, Y. Cui, B. Chen, B. Li and G. Qian, *Angew. Chem., Int. Ed.*, 2025, e202506055, DOI: **10.1002/anie.202506055**.
58 E. Wu, X. W. Gu, D. Liu, X. Zhang, H. Wu, W. Zhou, G. Qian and B. Li, *Nat. Commun.*, 2023, **14**, 6146.
59 H. Yang, Y. Wang, R. Krishna, X. Jia, Y. Wang, A. N. Hong, C. Dang, H. E. Castillo, X. Bu and P. Feng, *J. Am. Chem. Soc.*, 2020, **142**, 2222–2227.
60 S. Geng, E. Lin, X. Li, W. Liu, T. Wang, Z. Wang, D. Sensharma, S. Darwish, Y. H. Andaloussi, T. Pham, P. Cheng, M. J. Zaworotko, Y. Chen and Z. Zhang, *J. Am. Chem. Soc.*, 2021, **143**, 8654–8660.
61 H. Zhao, S. Guo, X. Chen, J. Jiang, S. Wang, H. Zhang, Y. Wang, X. He, M. Chen, W. Wang, S. Wang, P. Liu, H. Dai and M. Zhang, *Inorg. Chem.*, 2024, **63**, 7113–7117.
62 Y.-Z. Li, G.-D. Wang, R. Krishna, Q. Yin, D. Zhao, J. Qi, Y. Sui and L. Hou, *Chem. Eng. J.*, 2023, **466**, 143056.
63 G. D. Wang, Y. Z. Li, W. J. Shi, L. Hou, Y. Y. Wang and Z. Zhu, *Angew. Chem., Int. Ed.*, 2023, **62**, e202311654.
64 G. D. Wang, Y. Z. Li, R. Krishna, W. Y. Zhang, L. Hou, Y. Y. Wang and Z. Zhu, *Angew. Chem., Int. Ed.*, 2024, **63**, e202319978.
65 J. Xiao, Z. Zhu, M. Zhang, Y. Huang, T. C. Zhang and S. Yuan, *ACS Appl. Mater. Interfaces*, 2025, **17**, 21630–21642.
66 G. D. Wang, Y. Z. Li, H. Zeng, L. Hou, W. Lu and D. Li, *Adv. Funct. Mater.*, 2025, 2504916.
67 J. Li, Z. Song, X. Zhou, X. Wang, M. Feng, D. Wang and B. Chen, *Chem. Sci.*, 2025, **16**, 7411–7417.
68 S.-R. Liu, H.-Y. Duan, L.-F. Wu, J.-H. Zhao, Y.-J. Wang and X.-Y. Li, *Sep. Purif. Technol.*, 2025, **363**, 132190.

69 J. Peng, X. Zhang, R. Qin, F. Lai, N. Shi, Q. Ren and K. Chai, *Microporous Mesoporous Mater.*, 2025, **390**, 113600.
70 Q.-Q. Yang, Z.-H. Ma, Q. Zhang, Z.-H. Song, H.-X. Nie, J.-J. Pang, Z.-Q. Yao, H. Huang, M. Feng, T.-L. Hu and J. Xu, *Sep. Purif. Technol.*, 2025, **363**, 132141.
71 X. Ding, W. Wang, S. Guo, S. Wang, M. Chen, X. He, H. Zhao, J. Jiang, Y. Wang, Y. Liu, R. He, L. Han and M. Zhang, *Inorg. Chem.*, 2025, **64**, 2170–2175.
72 X.-Z. Guo, X.-X. Zhang, W. Liu, N. Ma, W. Xu, Y. Xu, Z. Xing, R. Krishna and J. Chang, *Sep. Purif. Technol.*, 2025, **361**, 131644.
73 L. Zhang, R. C. Gao, X. Liu, B. Zhang, L. Hou and Y. Y. Wang, *Adv. Funct. Mater.*, 2025, 2420927.
74 Z. Bao, S. Alnemrat, L. Yu, I. Vasiliev, Q. Ren, X. Lu and S. Deng, *Langmuir*, 2011, **27**, 13554–13562.
75 G. Chang, M. Huang, Y. Su, H. Xing, B. Su, Z. Zhang, Q. Yang, Y. Yang, Q. Ren, Z. Bao and B. Chen, *Chem. Commun.*, 2015, **51**, 2859–2862.
76 K. Li, D. H. Olson, J. Seidel, T. J. Emge, H. Gong, H. Zeng and J. Li, *J. Am. Chem. Soc.*, 2009, **131**, 10368–10369.
77 C. Y. Lee, Y. S. Bae, N. C. Jeong, O. K. Farha, A. A. Sarjeant, C. L. Stern, P. Nickias, R. Q. Snurr, J. T. Hupp and S. T. Nguyen, *J. Am. Chem. Soc.*, 2011, **133**, 5228–5231.
78 Y. Wang, N. Y. Huang, X. W. Zhang, H. He, R. K. Huang, Z. M. Ye, Y. Li, D. D. Zhou, P. Q. Liao, X. M. Chen and J. P. Zhang, *Angew. Chem., Int. Ed.*, 2019, **58**, 7692–7696.
79 Y. Chen, H. Wu, L. Yu, S. Tu, Y. Wu, Z. Li and Q. Xia, *Chem. Eng. J.*, 2022, **431**, 133284.
80 L. Li, F. Xiang, Y. Li, Y. Yang, Z. Yuan, Y. Chen, F. Yuan, L. He, S. Xiang, B. Chen and Z. Zhang, *Angew. Chem., Int. Ed.*, 2025, **64**, e202419047.
81 M. Bonneau, K. Sugimoto, K. i. Otake, Y. Tsuji, N. Shimanaka, C. Lavenn and S. Kitagawa, *Nat. Sci.*, 2021, **1**, e10020.
82 H. Xiong, Y. Peng, X. Liu, P. Wang, P. Zhang, L. Yang, J. Liu, H. Shuai, L. Wang, Z. Deng, S. Chen, J. Chen, Z. Zhou, S. Deng and J. Wang, *Adv. Mater.*, 2024, **36**, e2401693.
83 H.-P. Li, J.-W. Wang, Z. Dou, L.-Z. Wu, Y. Wang, Y. Liang and Q.-G. Zhai, *Chem. Eng. J.*, 2024, **492**, 152125.
84 W. Zhang, S. Zou, Y. Zhou, Z. Ji, H. Li, G. Zhen, C. Chen, D. Song and M. Wu, *Inorg. Chem.*, 2024, **63**, 3145–3151.
85 H. Fang, X. Y. Liu, H. J. Ding, M. Mulcair, B. Space, H. Huang, X. W. Li, S. M. Zhang, M. H. Yu, Z. Chang and X. H. Bu, *J. Am. Chem. Soc.*, 2024, **146**, 14357–14367.